

Automatic detection and measurement of nuchal translucency



Giuseppa Sciortino^a, Domenico Tegolo^{a,b,c}, Cesare Valenti^{a,*}

^a Dipartimento di Matematica e Informatica, Università degli Studi di Palermo, Italy

^b Centro Interdipartimentale di Tecnologie della Conoscenza, Università degli Studi di Palermo, Italy

^c Mediterranean Center for Human Health Advanced Biotechnologies, Palermo, Italy

ARTICLE INFO

Keywords:

Nuchal translucency
Ultrasound fetal examination
Wavelet analysis
Median sagittal section
First trimester of pregnancy

ABSTRACT

In this paper we propose a new methodology to support the physician both to identify automatically the nuchal region and to obtain a correct thickness measurement of the nuchal translucency. The thickness of the nuchal translucency is one of the main markers for screening of chromosomal defects such as trisomy 13, 18 and 21. Its measurement is performed during ultrasound scanning in the first trimester of pregnancy. The proposed methodology is mainly based on wavelet and multi resolution analysis. The performance of our method was analysed on 382 random frames, representing mid-sagittal sections, uniformly extracted from real clinical ultrasound videos of 12 patients. According to the ground-truth provided by an expert physician, we obtained a true positive rate equal to 99.95% with respect to the nuchal region detection and about 64% of measurements present an error equal to 1 pixel (which corresponds to 0.1 mm), respectively.

1. Introduction

Down's Syndrome (namely DS), identified in 1886 by Dr. Langdon Down, is a genetic condition that causes a variable degree of delay in mental, physical and motor development. It is caused by the presence of an extra chromosome in the nucleus of every cell (47 in comparison with a normal number of 46) in the twenty-first pair; for this reason DS is often indicated as trisomy 21. Its causes are still unknown and therefore there is no real way of prevention. Early in the 70's, the maternal age was the first element to deduce the probability for the fetus to present a chromosomal defect.

During the last few years it has been demonstrated [1,2] that there is a correlation between DS and some ultrasound and biochemical markers. Maternal age and biochemical markers present in maternal serum (dosages of Free Beta-HCG and Papp-A) are used to identify about 50–70% of fetuses affected by DS [3]. Due to the study of sonographic markers such as nuchal translucency (NT) it is possible to achieve a better detection rate of 90%, which increases to 95% when analysing also the nasal bone. These examinations provide a good alternative to invasive tests, such as amniocentesis (i.e. the analysis of the amniotic liquid) and chorionic villus sampling, which present a greater accuracy but introduce a risk of miscarriage or fetal injury of 2% and 1% for the chorionic villus sampling and amniocentesis [4,5] respectively. Amniocentesis should be performed between the fourteenth and twentieth week of gestation and it is associated with an increased risk of respiratory distress syndrome and pneumonia, while

chorionic villus sampling, which may cause general birth defects, should not be performed before the eleventh week.

Nuchal translucency (see Fig. 1) is a fluid fill under the necks skin of the fetus which appears sonographically as an anechogenic area (i.e. a dark zone in greyscale images) between two echogenic regions (i.e. bright zones). The thickness of the nuchal translucency, also called the diameter, is related not only to DS, but also to other genetic abnormalities such as Edwards' (trisomy 18), Palau's (trisomy 13), Turner's syndromes and defects related to the heart [6]. The optimal period to measure the NT thickness lies between the eleventh and the thirteenth weeks, when the NT reaches the maximum thickness, then after this period tends to disappear. During this period it also possible to verify other eventual complications, including miscarriage, stillbirth, preeclampsia, gestational diabetes mellitus, preterm delivery, fetal growth restriction and macrosomia (Table 1).

The measurement of the NT requires non-trivial sonographer skills and the Fetal Medicine Foundation (FMF) has drawn up a protocol about these requirements in order to ensure correct measurement. The purpose of this article is to propose an effective tool to support early diagnosis by the automatic measurement of NT; the proposed methodology is able to automatically locate the neck region, to identify the nuchal translucency and to measure its thickness without any user intervention, thus obviating the inter- and intra- observer variabilities.

* Corresponding author.

E-mail addresses: giuseppa.sciortino04@unipa.it (G. Sciortino), domenico.tegolo@unipa.it (D. Tegolo), cesare.valenti@unipa.it (C. Valenti).

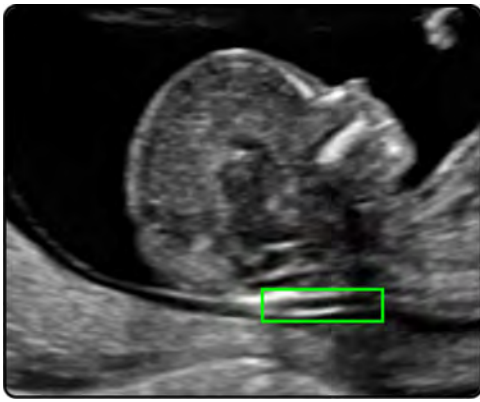


Fig. 1. The green rectangle indicates the hyperechogenic regions that delimit the nuchal transluency.

Table 1
Nomenclature and variables.

DS	down's Syndrome, also known as trisomy 21
NT	nuchal transluency
FMF	Fetal Medicine Foundation
H.264	moving Picture Experts Group 4 Part 10 Advanced Video Coding
μ	mean of the values of a given image
σ	standard deviation of the values of a given image
I	input greyscale image
ℓ_i	level i of the low-pass kernel of the <i>à trous</i> algorithm
\mathbf{q}	generic pixel that spans ℓ_i
\mathbf{p}	generic pixel that spans a given image
I_i	level i of the convolution of the <i>à trous</i> algorithm
W_i	level i of the wavelet coefficients of the <i>à trous</i> algorithm
C	thresholded version of W_i only
B_i	thresholded version of W_i
k	parameter to threshold W_i in B_i
B	image composition of $B_{4,5,6}$ through voting strategy
$A(A_x, A_y)$	coordinates of the leftmost upper pixel of the nuchal transluency bounding box
$B(B_x, B_y)$	coordinates of the rightmost lower pixel of the nuchal transluency bounding box
(X, Y)	coordinates of the centre of the circle that inscribes the head
R	radius of the circle that inscribes the head
M	abscissa of the rightmost pixel of the mandible
D_r	discrete disk with radius r pixels
ϵ_r	mathematical morphology erosion with structuring element D_r
δ_r	mathematical morphology dilation with structuring element D_r
ρ	mathematical morphology edge detector

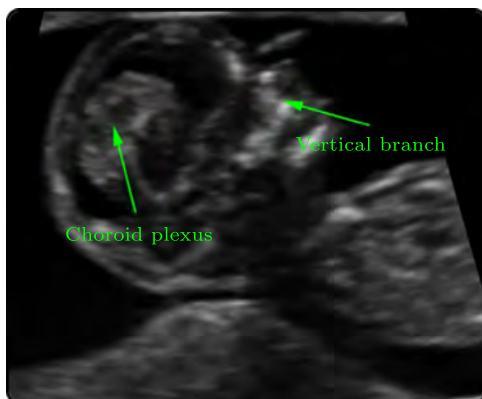


Fig. 2. The presence of the vertical branch of the jaw bone and the choroid plexus indicates that the considered section is not mid-sagittal.

2. Related work

In the literature there are several works about the measurement of NT; in particular Bernardino et al. [7] is one of the first works that

attempted to automate the procedure. Their procedure is semi-automatic because the user has to identify by hand the membranes that surround the translucency: they represent the starting points which will be tracked through the edges by Sobel and Canny filters.

A semi-automatic method proposed by Lee et al. [8] is based on dynamic programming and on a non-linear anisotropic filter [9] to reduce eventual speckle noise. This method tends to underestimate the thickness of the NT with respect to the ground truth provided by a physician. Furthermore the applicability of the procedure is limited to images in which the fetus is in a horizontal position.

Catanzariti et al. [10] proposed a method based on dynamic programming; they significantly improved the cost function for the segmentation of the edges which delimit the translucency. Indeed, it does not require any initial parameter, the process is applicable without the intervention of the user, and the selection of the initial points to detect the edges is not necessary. A qualitative analysis showed the efficiency of the method.

In Nirmala et al. [11], images are pre-processed by applying a median filter to remove speckle noise. The user identifies the region in which the NT is present and the mean shift algorithm for segmentation is applied on that region. Subsequently the Canny operator is applied on the segmented images to extract the edges which delimit the NT. A blob analysis is proposed for measuring the thickness of the translucency. The authors report a quantitative comparison between the mean values of thicknesses of the translucency considered normal and abnormal.

In Deng et al. [12] a semi-automatic scheme is proposed: the images are pre-processed by morphological filtering to reduce noise and subsequently a threshold is applied with a value calculated empirically. The user selects two initial points and the edges are located starting from them by a gradient vector flow snake approach; the edges thus obtained are improved by means of a dynamic programming algorithm. Finally the thickness and the area of the NT are calculated. The authors show a qualitative comparison of the results on synthetic and real data.

A hierarchical model for the automatic identification of the nuchal region is proposed in Deng et al. [13]: three support vector machine classifiers are trained to represent the neck region, the head and the body of the fetus. In Deng et al. [14] the same method was revisited by adding another level of the hierarchical model to represent the fetal profile and with improved performance.

Although the technical details were not disclosed, in Moratalla et al. [15] the tool called SonoNT is presented: it is already integrated and commercialized in some ultrasound devices and it allows a semi-automatic measurement of the nuchal transluency which has to be delimited by the user in a box so as to contain the maximum thickness of the NT. The tool tracks the top and bottom edges using the information of the gradient and brightness inside the box and finally it identifies the maximum vertical distance between these two edges.

An automated method to detect and to measure the NT is presented in Supriyanto et al. [16]: the region containing the nuchal transluency is identified with a multilayer neural network which processes sub-samples of the image and returns the degree of belonging to the class representative of the nuchal transluency. Once the points with a higher probability of belonging to the nuchal transluency region are identified, the methodology draws the edges with an automatic algorithm based on intensity measurements, known as “bidirectional iterations propagations forward method”. This approach relies on a preliminary manual classification of the mid-sagittal sections and the final results are based on a correlation index between the average observations provided by a physician and their corresponding automatic measurements.

In 2013, Park et al. [17] proposed a methodology to measure the NT automatically; first the position of the head is identified and then the neck region is located by statistical relationships between them. Dijkstra's algorithm is applied to locate the inner and outer edges of the

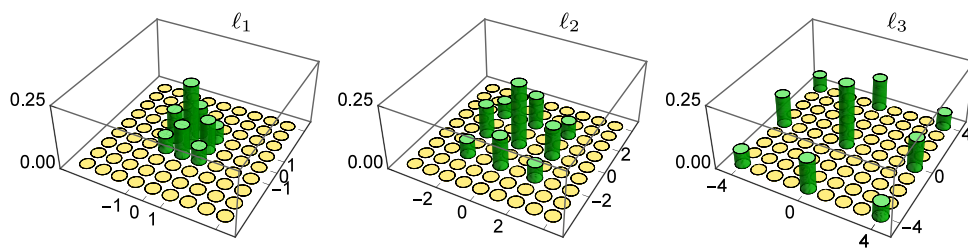


Fig. 3. Graphic representation of the first three kernels ℓ_1 , ℓ_2 and ℓ_3 . The values of non-zero elements are depicted in green.



Fig. 4. The cisterna magna (highlighted by the arrow) usually shows characteristics quite similar to those of the translucency of Fig. 1.

two components which delimit the translucency; the seed points are chosen within these regions and the segmentation graph cut algorithm is applied; finally, the diameter of the NT is measured. Qualitative assessments for the extraction of the edges and the thickness of translucency are shown graphically, proposing the five best and worst cases.

The semi-automatic methodology proposed by Sonia et al. [18] aims to classify the thickness of the (normal and abnormal) nuchal translucency by using a support vector machine. The feature extraction is performed by applying a discrete wavelet transform. In that methodology the NT thickness is not measured quantitatively, the edges are not drawn, and the maximum diameter is not measured.

To the best of our knowledge all these works provide qualitative assessments or show average values that do not allow a direct comparison with our results.

Anzalone et al. [19] show a study dedicated to the automatic identification of the sagittal median and NT measurement. The methodology consists of two stages: the former identifies the medial sagittal sections, the latter searches the nuchal region and measures the NT thickness. The chin is identified by template matching to determine

the fetal profile, useful for the identification of the NT which takes place again by a template matching; finally, the procedure proposed in [10] is applied for edges extraction. Experiments were performed to determine the best metric for the template matching and to compute the correct number of templates required for the identification of the chin and the nuchal translucency.

3. Materials and methods

Unfortunately, no public domain repository with medical records is available to allow direct comparisons among various approaches. In order to verify the robustness of our methodology we created a dataset of images according to the protocol drawn up by the Fetal Medicine Foundation [6], directed to skilled sonographers who are proven to have an excellent technical knowledge for measuring the NT. The following statements of the protocol for measurement, presented in <https://fetalmedicine.org/nuchal-translucency-scan>, are closely related to the aims of our methodology:

- the gestational period must be the eleventh and the thirteenth weeks and six days;
- the fetal crown-rump length should be between 45 and 84 mm;
- the magnification of the image should be such that the fetal head and thorax occupy the whole screen;
- a mid-sagittal view of the face should be obtained. Minor deviations from the exact midline plane would cause non-visualization of the tip of the nose and visibility of the zygomatic process of the maxilla;
- the fetus should be in a neutral position, with the head in line with the spine. When the fetal neck is hyperextended the measurement can be falsely increased and when the neck is flexed, the measurement can be falsely decreased;
- care must be taken to distinguish between fetal skin and amnion;
- the widest part of translucency must always be measured;
- measurements should be taken with the inner border of the horizontal line of the callipers placed on the line that defines the nuchal translucency thickness – the crossbar of the calliper should be such that it is hardly visible as it merges with the white line of the



Fig. 5. The main components can be located according to the procedure described in [20] and to refine the bounding box by considering only the bigger component ascribable to the nuchal translucency (right), thus obtaining the result of Fig. 1.

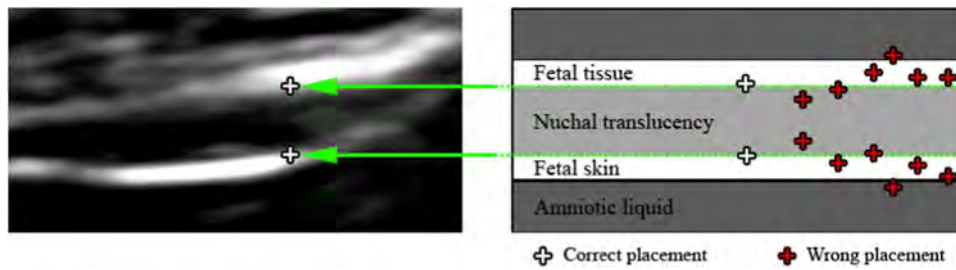


Fig. 6. Calliper positioning in order to measure the diameter of the nuchal translucency, which is the maximum length within the nuchal area.

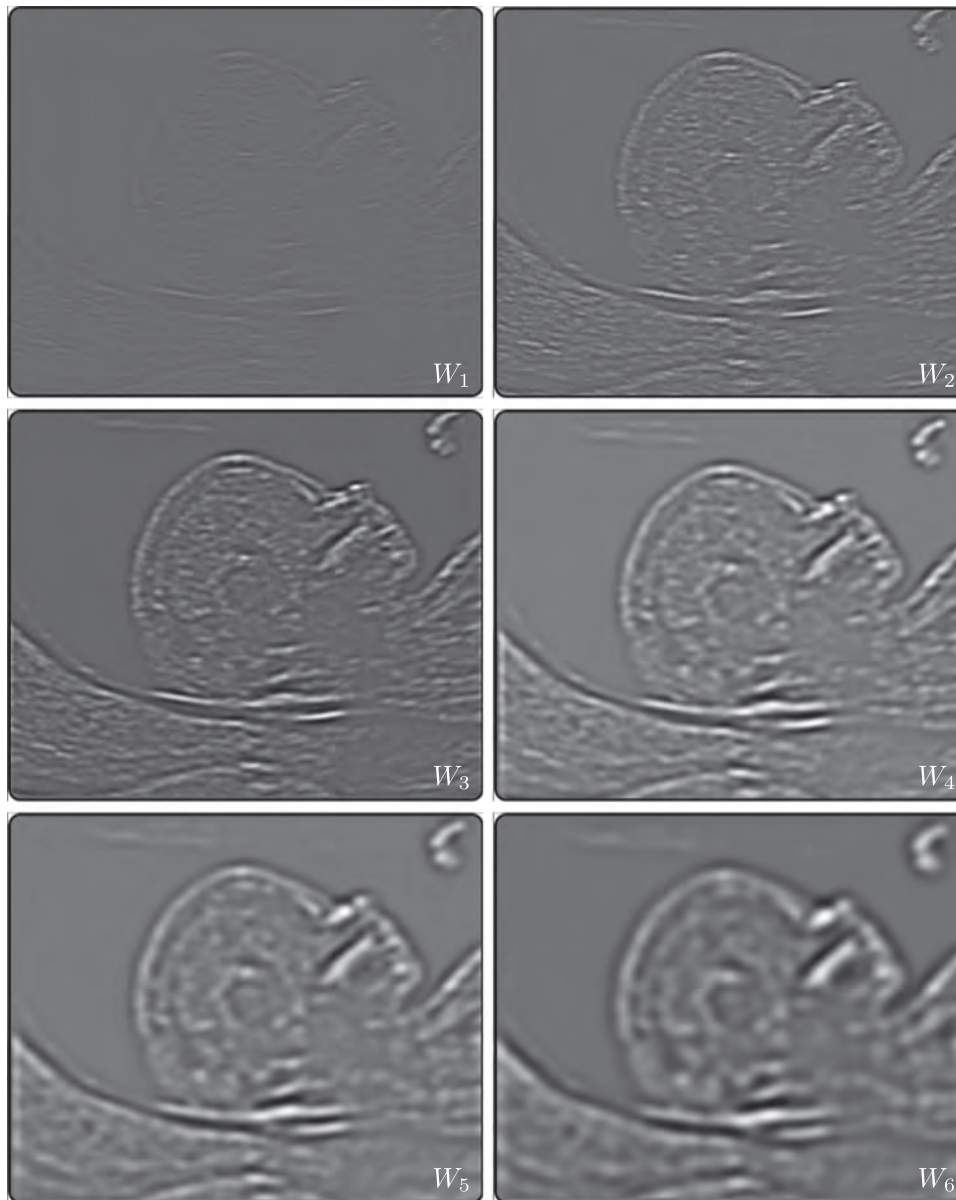


Fig. 7. The first six wavelet planes $W_1 \dots W_6$ contains structures with lower and lower frequencies.

border, not in the nuchal fluid.

The protocol drawn up by the FMF has been considered in this work. The images in the analysis represent median sagittal sections determined by the automatic algorithm implemented in [20] which locates and processes both the jaw bone and the choroid plexus (Fig. 2).

3.1. Dataset description

To develop and to evaluate our methodology we involved subjects between the 11th and the 13th weeks of pregnancy. An expert physician used a GE Voluson E8 equipment to acquire sagittal sections showing the left or the right profile of the head and we selected 382 ultrasound mid-sagittal sections by using the approach described in [20]. To avoid as many artifacts as possible, all files were stored with

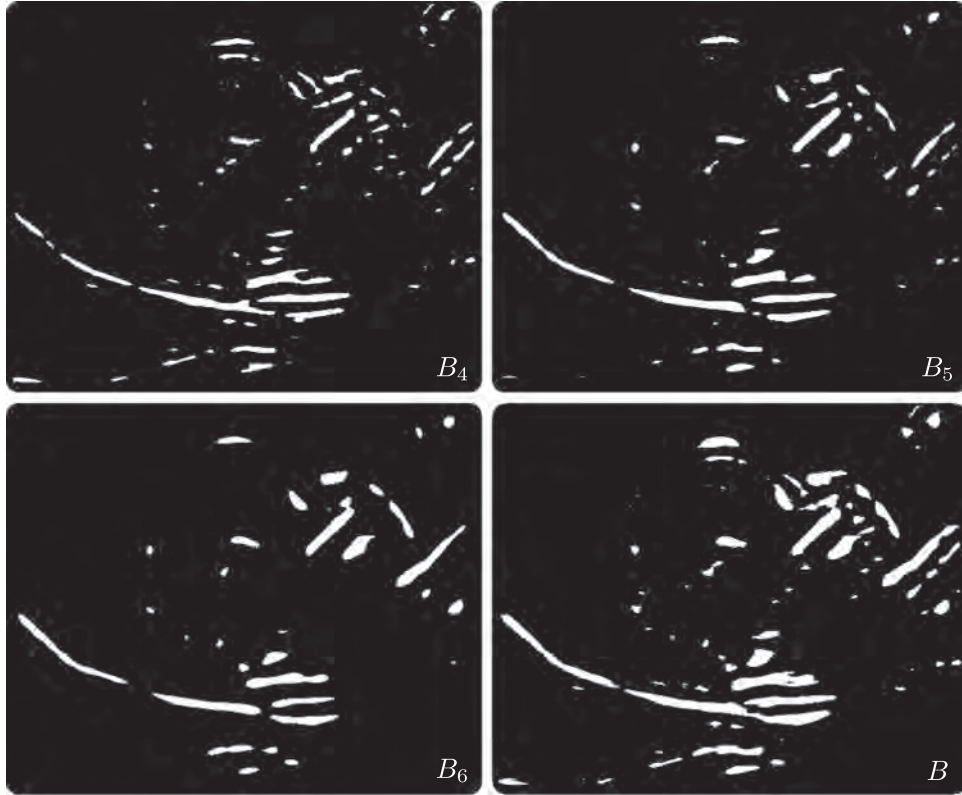


Fig. 8. We combine just the binarized wavelet planes B_4 , B_5 and B_6 to obtain the enhanced mask B which contains most of the useful components.

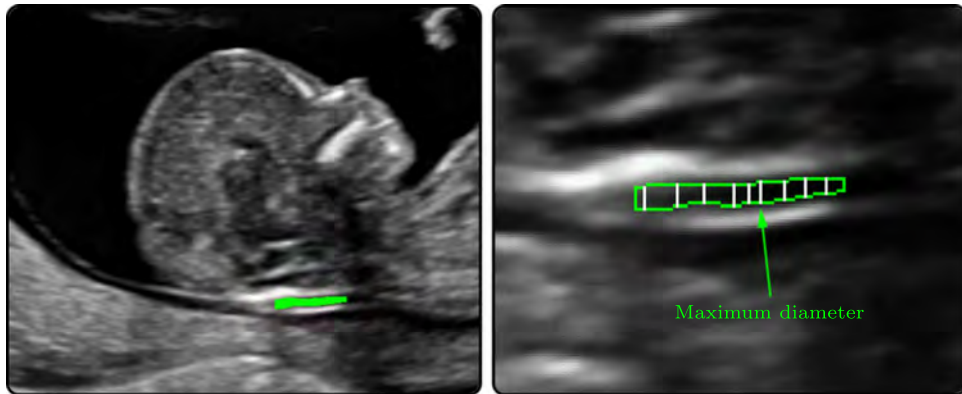


Fig. 9. Detected nuchal translucency and its zoom. The contour of the nuchal translucency is coloured in green, while some representatives of its diameters are in white. The maximum diameter is highlighted by the arrow.

the lowest compression ratio of the H.264 codec (formally ISO/IEC 14496-10 by International Telecommunication Union, 2013) and each frame was saved in the Portable Network Graphics lossless format with 640×480 pixels, where a pixel corresponds to a resolution of 0.1 mm.

3.2. Wavelet image processing

Wavelet analysis is a well-known mathematical tool used in the field of signal processing to extract information from different kinds of data through convolutions with opportunely scaled wavelet functions. From a practical viewpoint this process is called a filterbank and consists in a succession of low-pass and high-pass filters on the input signal. We verified the appropriateness of different wavelet transforms and functions, though we will report here only the most promising approach able to solve our particular task.

We preferred the so-called *à trous* algorithm [21] because it retains the maximum resolution with respect to the usual multiresolution

analysis [22], which gives rise to a reduced representation: while the former method produces wavelet planes of the same size as the original image (therefore useful for image segmentation), the latter returns wavelet planes of decreasing sizes (consequently suited for image compression).

In order to highlight details in the image, it is necessary to apply a compact kernel as described in [23]:

$$\ell = \frac{1}{16} \begin{bmatrix} 1 & 2 & 1 \\ 2 & 4 & 2 \\ 1 & 2 & 1 \end{bmatrix} \quad (1)$$

which is isotropic and can be speeded up through the Kronecker product:

$$\ell = \frac{1}{16} \begin{bmatrix} 1 \\ 2 \\ 1 \end{bmatrix} \otimes [1 \ 2 \ 1]. \quad (2)$$

Bigger structures require a kernel with comparable size to be

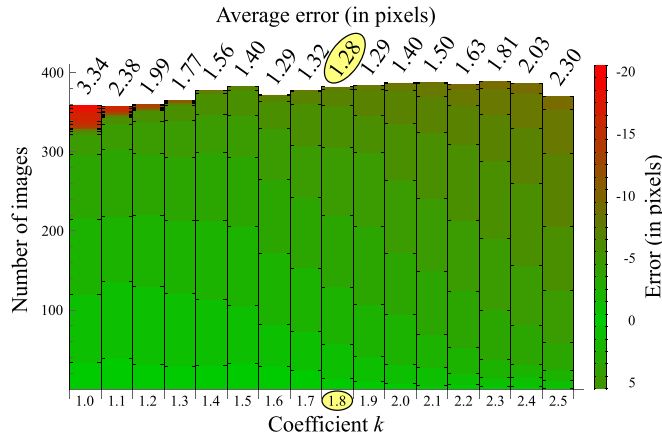


Fig. 10. Distribution of the number of still frames with a given error (indicated by the vertical legend) due to the automatic methodology, with respect to the coefficient k . Best values are pointed out in yellow. The reader is referred to the electronic version of the article for interpretation of the colours in this figure.

located; this can be obtained by creating a sparse representation of ℓ :

$$\ell_i(2^{i-1}\mathbf{q}) = \ell(\mathbf{q}) \quad (3)$$

where the pixel \mathbf{q} spans the 3×3 original kernel ℓ and the distance between non-zero elements is equal to a power of 2. The remaining elements of ℓ_i are set to zero (Fig. 3). In other words, the number of non-zero elements in ℓ_i is constant and therefore this wavelet algorithm always takes the same time to compute the following series of convolutions:

$$I_0(\mathbf{p}) = I(\mathbf{p}), \quad I_i(\mathbf{p}) = I_{i-1}(\mathbf{p}) \otimes \ell_i \quad (4)$$

where \mathbf{p} indicates the position of a generic pixel of the input image I .

Recalling that I_i are smoother and smoother images, a simple high-pass filter is defined as the difference between two consecutive planes, which contains components with specific frequencies (i.e. size):

$$W_i(\mathbf{p}) = I_{i-1}(\mathbf{p}) - I_i(\mathbf{p}). \quad (5)$$

Small objects are enhanced in the first planes W_1 and W_2 , while bigger components are located in the successive planes.

3.3. Nuchal bounding box detection

The proposed methodology is composed of two main steps: identification and measurement of the nuchal translucency. The NT is an anechogenic region and it is delimited by two components that are more echogenic than it. The upper component is always easily detectable because its echogenicity is usually greater. Unfortunately, the lower component is not always easily identifiable. On the other hand, the NT thickness between these two regions is always anecho-

genic although it should be noted that in its proximity other strongly anechogenic structures (for example, in the case of the cisterna magna) may be present (Fig. 4).

We apply the wavelet transform to segment the images by setting the thresholding value according to the following equation:

$$C(\mathbf{p}) = \{\mathbf{p}: W_6(\mathbf{p}) > \mu(W_6) + 2\sigma(W_6)\} \quad (6)$$

where μ and σ indicate the mean and the standard deviation of the values of a given wavelet plane. Our experiments proved that this simple approach is quite effective, at least with our images, and it is not necessary to apply more complex techniques as described, for example, in [24,25] due to the fact that the wavelet transform is able to reduce the effect of eventual speckle noise deleted in the first planes W_1 and W_2 .

In the mid-sagittal sections there are some structures with similar characteristics with respect to the nuchal translucency and for this reason we limit the search area by considering the geometric relationships among the jaw bone and the nuchal translucency. Starting from the centre of the maximal circumference that inscribes the head of the fetus, obtained by a modified version of the fast radial symmetry transform described in [26], we locate a rough bounding box $[A, B]$ which represents the nuchal translucency (Fig. 5). In order to obtain this box we rely on the following spatial relationships, which were formulated on average according to anatomical observations:

$$A_x = X, \quad A_y = Y - 1.5R, \quad B_x = M, \quad B_y = Y - 2.0R \quad (7)$$

where (X, Y) are the coordinates of the centre of the circle located by the symmetry transform and R indicates its radius. M corresponds to the rightmost point of the mandible.

We therefore refine the size and the position of the region of interest, by considering the jaw bone and the component with the maximal area within this box. Fig. 5 depicts both the preliminary zone of interest, further refined on $C(\mathbf{p})$ to include only the nuchal translucency.

3.4. Measurement of the nuchal translucency

Once the nuchal region is identified, the focus is on the nuchal translucency and the two regions that delimit it. It is necessary to distinguish between the fetal skin and amnion, which both appear as thin membranes. The calliper, as specified by the protocol, should be placed on the lines that define the NT thickness, paying attention not to place them in the nuchal fluid. Fig. 6 sketches possible cases of correct and incorrect positioning of the calliper.

Generally the structures in ultrasound images do not have well-defined edges and, in the specific case of the nuchal translucency, the brightness plays an important role because of many and sudden changes of brightness (for example, due to the speckle noise). This step of the proposed method is based again on the use of information

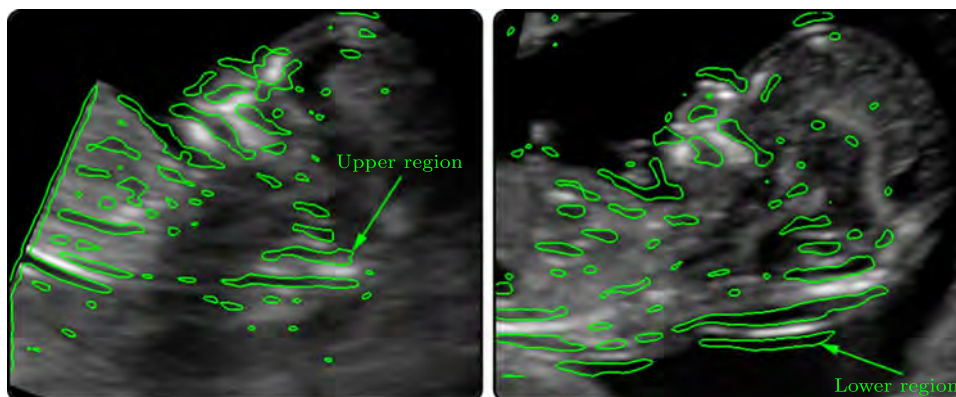


Fig. 11. Upper and lower anechogenic regions with respect to the position of the nuchal translucency.

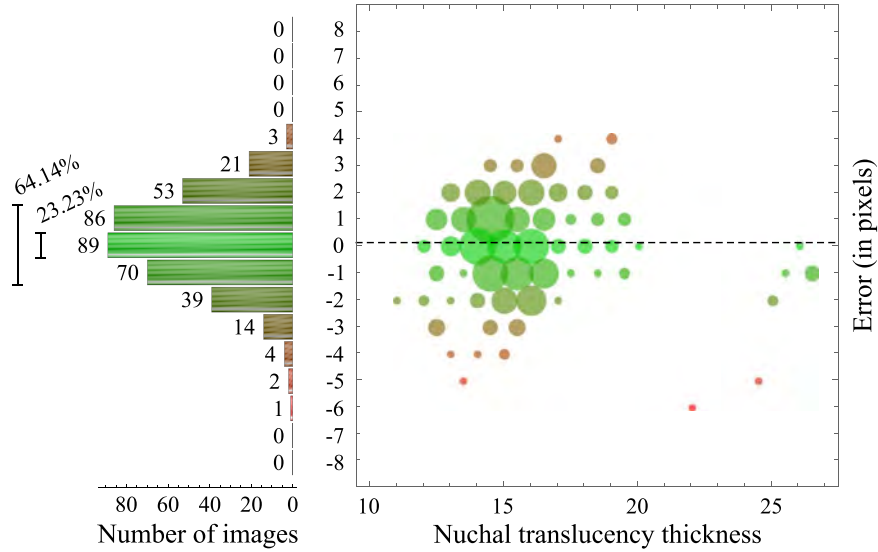


Fig. 12. Error distribution with respect to the thickness of the nuchal translucency. The area of each disk indicates the number of images. The average error, represented by the dashed line, is equal to 0.118 pixels (i.e. 0.0118 mm), which means an equal number of under- and over-estimated measurements. In particular, the histogram shows that about 23.23% and 64.14% of the 382 images present an error equal to 0 or ± 1 pixels (i.e. 0.1 mm), respectively.

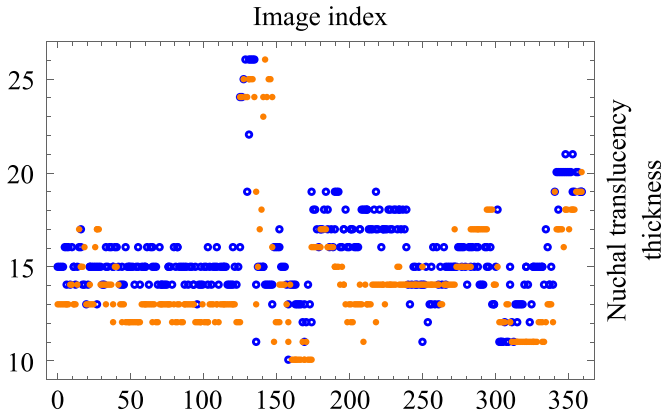


Fig. 13. Comparison between the automatic measurement (blue circles) and the manual ground truth (orange disks) for each image.

extracted through the wavelet transform at different scales. The input image is preliminarily decomposed into frequency bands, according to the paradigms of the multi-resolution analysis. Information about the edges is then propagated between the various scales: the edges at high frequencies may appear segmented and instead be contiguous at the low frequencies.

Individually, the binary masks do not ensure a good compromise between the extension of the components and the definition of the edges. This is due to the high variability (in brightness, but also in noise) of the ultrasound images, and for this reason the binary masks obtained from consecutive planes are joined together in a new binary mask that includes the information coming from different scales. This technique preserves the dimensions of the components and maintains at the same time a sufficient level of detail from the high frequencies. The entire procedure is robust even with speckle noise, ensuring components with entire and continuous edges. In particular, the planes W_4 , W_5 and W_6 (Fig. 7) are chosen and, analogously to Eq. (6), we apply the following threshold (with $k=1.8$, identified experimentally as described in Section 4.1) to get the binary masks B_4 , B_5 and B_6 (Fig. 8).

$$B_i(\mathbf{p}) = \{p: W_i(\mathbf{p}) > \mu(W_i) + k\sigma(W_i)\} \quad (8)$$

Then the masks B_i are combined together through a voting strategy which considers at least two out of three pixels to return the main structures (Fig. 8).

$$B(\mathbf{p}) = \left\{ p: \sum_{i=4}^6 B_i(\mathbf{p}) \geq 2 \right\} \quad (9)$$

Taking into account the bounding box of Fig. 5, we label as nuchal translucency the bigger component of B which falls within that box. We verified that the mathematical morphology ρ operator with a structuring element defined by the discrete disk D_1 of radius equal to one pixel is able to enhance effectively the edges in the binary image (Fig. 9) [27]:

$$\rho(B(\mathbf{p})) = \delta_1(B(\mathbf{p})) - \varepsilon_1(B(\mathbf{p})) \quad (10)$$

where

$$\varepsilon_r(B(\mathbf{p})) = \min_{\mathbf{q} \in D_r} B(\mathbf{p} + \mathbf{q}), \quad \delta_r(B(\mathbf{p})) = \max_{\mathbf{q} \in D_r} B(\mathbf{p} + \mathbf{q}). \quad (11)$$

The diameter is defined as the distance between the pixels belonging to the lower and upper edges; the maximum diameter, according to the FMF protocol, corresponds to the measure to be associated with the considered frame (Fig. 9).

4. Results and discussions

The methodology is based on both the detection and the measurement of the nuchal translucency. Although of some methods have already been proposed in the literature, only a few of them can be considered fully automatic and moreover none of them obtained the expected results. The first phase of our methodology regards the detection of the translucency; the second phase regards the measurement and we will report details about the agreement with an expert physician upon real clinical examinations.

4.1. Proper threshold selection

A quantitative analysis of the binary masks obtained by the wavelet planes allows us to identify the best value of the parameter k (cf. (8)) to minimize the average error of the automatic measurement in comparison with the manual annotation and to maximize the number of frames that present a wrong diameter not exceeding that average error. It follows that a suitable value is $k=1.8$, which corresponds to an average error of about 1.28 pixels (i.e. 0.128 mm). Both these values are highlighted in Fig. 10.

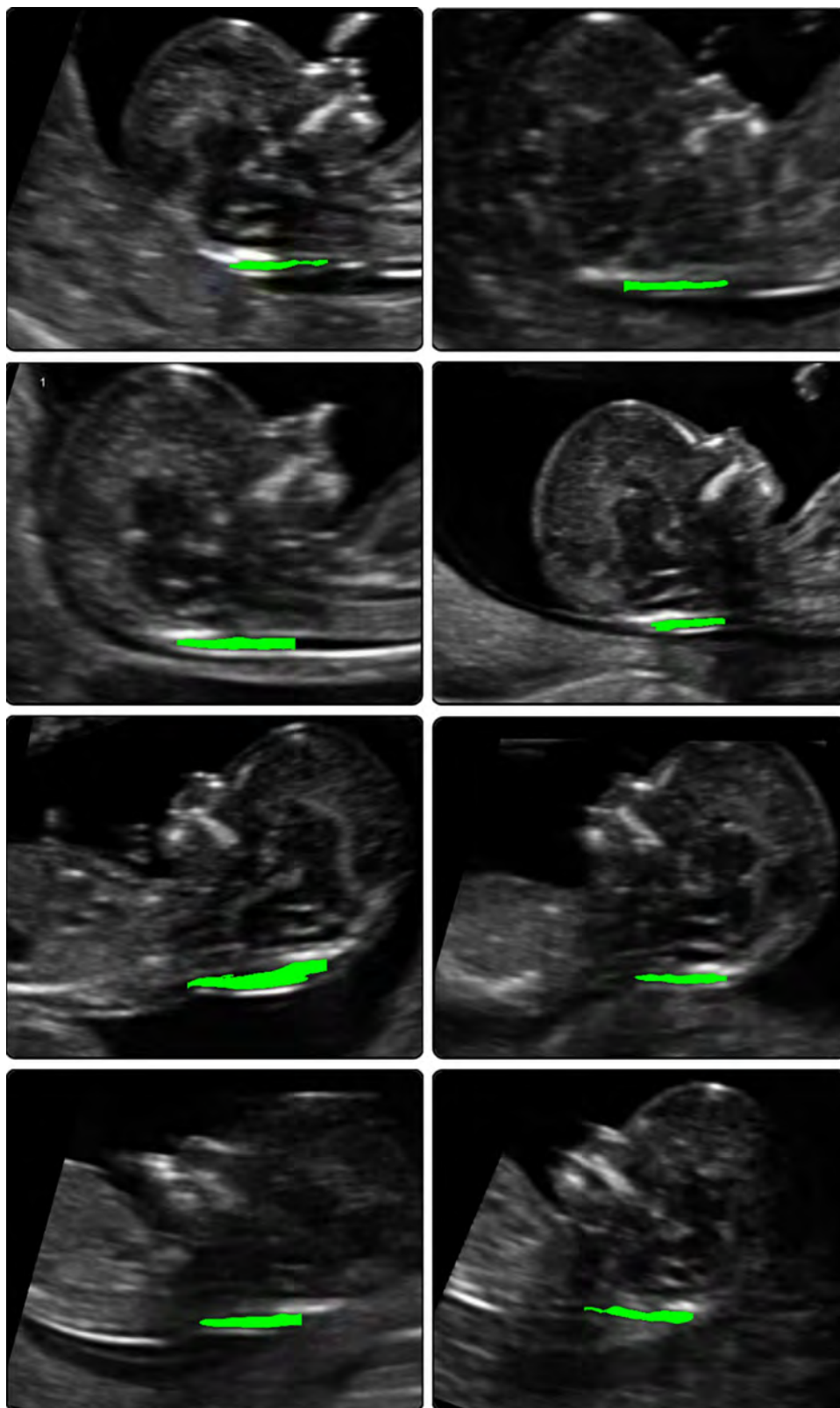


Fig. 14. The area of the nuchal translucency identified by our methodology is highlighted in green.

4.2. Nuchal region and thickness evaluation

Occasionally, the nape region is erroneously detected because regions close to it can manifest similar morphological and echogenic characteristics in the upper zone of the nuchal translucency, as in the case of the cisterna magna, or in the lower area, as in the case of the

amniotic sac (Fig. 11). The overall correct identification rate is equal to 99.95%, obtained by counting the number of nuchal regions correctly detected by the system with respect to the judgment by the expert physician.

Fig. 12 shows the frequency distribution of the images with a given error versus the manual measurement. The more circles lie on an error

equal to zero, the better it is. In particular 23.23% of the solutions present an error equal to zero pixels; 64.14% of the solutions present an error up to one pixel (i.e. 0.1 mm), which is in good accordance with the physician's evaluation. An in-depth comparison for each single image is given in the Bland-Altman plot of Fig. 13. Fig. 14 shows some examples to give a qualitative assessment.

5. Conclusions

The proposed contribution introduces an automatic methodology to support physicians in the evaluation of some important chromosomal defects. It must be stressed that, according to the international acquisition protocol described in [6], only mid-sagittal sections must be considered. Indeed, our methodology relies on the selection of those frames from video sequences, due to our algorithm already described in [20]. Here we focus our attention on detecting and measuring the nuchal translucency, thus presenting a complete environment to highlight eventual diseases like trisomy 13, 18 and 21 during ultrasound scanning in the first trimester of pregnancy. We experimentally verified the correctness of our methodology on 382 random frames from 12 real examinations and compared the obtained results against the ground-truth provided by an expert physician. It must be noted that no public domain repository with medical records about nuchal translucency evaluations is available to compare various approaches. With respect to the nuchal region detection, we obtained a true positive rate equal to 99.95% and about 64% of measurements present an error equal to no more than 1 pixel, which corresponds to 0.1 mm. To the best of our knowledge most works in the literature provide qualitative assessments or show average values that do not allow a direct comparison with our results. We are aware that future screening procedures will be based more and more on the analysis of genetic information of the fetus, but our system can be employed right now on standard ultrasound equipment without any particular additional charges. We developed the whole system within the MatLab environment and it requires about 0.20 s to process each image with 640×480 pixels on an entry-level machine equipped with an Intel i5-2400@3.1 GHz, 4 GB RAM and Windows 7; therefore we expect that a real industrial version could be further optimized by embedding also a suitable user-friendly interface. Moreover, the ultrasound examination is repeatable, non-invasive and, with respect to chorionic villus sampling and amniocentesis, it does not present any risk of miscarriage or fetal injury.

Conflict of interest statement

The authors hereby declare that there is no conflict of interest with any organization.

Acknowledgement

We are grateful to Dr Emanuela Orlandi from Azienda Ospedaliera Universitaria Policlinico Paolo Giaccone of Palermo in Italy for providing the ultrasound dataset and its ground truth.

Appendix A. Supplementary data

Supplementary data associated with this article can be found in the online version at <http://dx.doi.org/10.1016/j.combiomed.2017.01.008>.

References

[1] K. Nicolaides, G. Azar, D. Byrne, C. Mansur, K. Marks, Fetal nuchal translu-

- ency: ultrasound screening for chromosomal defects in first trimester of pregnancy, *Br. Med. J.* 304 (6831) (1992) 867–869.
- [2] K. Nicolaides, M. Brizot, R. Snijders, Fetal nuchal translucency-ultrasound screening for fetal trisomy in the first trimester of pregnancy, *Br. J. Obstet. Gynaecol.* 101 (9) (1994) 782–786.
- [3] N. Wald, L. George, D. Smith, J. Densem, K. Pettersson, Serum screening for Down's syndrome between 8 and 14 weeks of pregnancy, *Br. J. Obstet. Gynaecol.* 103 (5) (1996) 407–412.
- [4] Z. Alfrevic, K. Sundberg, S. Brigham, Amniocentesis and chorionic villus sampling for prenatal diagnosis, *Cochrane Database of Systematic Reviews* 3.
- [5] A. Tabor, M. Madsen, E. Obel, J. Philip, J. Bang, B. Gaard-Pedersen, Randomised controlled trial of genetic amniocentesis in 4606 low-risk women, *Lancet* 327 (8493) (1986) 1287–1293.
- [6] FMF, Fetal Medicine Foundation nuchal translucency. (<http://www.fetalmedicine.org/>).
- [7] F. Bernardino, R. Cardoso, N. Montenegro, J. Bernardes, J. Marques De Sa, Semiautomated ultrasonographic measurement of fetal nuchal translucency using a computer software tool, *Ultrasound Med. Biol.* 24 (1) (1998) 51–54.
- [8] Y. Lee, M. Kim, M. Kim, Robust border enhancement and detection for measurement of fetal nuchal translucency in ultrasound images, *Med. Biol. Eng. Comput.* 45 (11) (2007) 1143–1152.
- [9] P. Perona, J. Malik, Scale-space and edge detection using anisotropic diffusion, *IEEE Trans. Pattern Anal. Mach. Intell.* 12 (7) (1990) 629–639.
- [10] E. Catanzariti, G. Fusco, F. Isgrò, S. Masecchia, R. Prevete, M. Santoro, A semi-automated method for the measurement of the fetal nuchal translucency in ultrasound images, in: *Proceedings of the International Conference on Image Analysis and Processing*, Vol. 5716 of *Lecture Notes in Computer Science*, Springer, 2009, pp. 613–622.
- [11] S. Nirmala, V. Palanisamy, Measurement of nuchal translucency thickness for detection of chromosomal abnormalities using first trimester ultrasound fetal images, *Int. J. Comput. Sci. Inf. Secur.* 6 (3) (2009) 101–106.
- [12] Y. Deng, Y. Wang, P. Chen, Estimating fetal nuchal translucency parameters from its ultrasound image, in: *Proceedings of the International Conference on Bioinformatics and Biomedical Engineering*, IEEE, 2008, pp. 2643–2646.
- [13] Y. Deng, Y. Wang, P. Chen, Automated detection of fetal nuchal translucency based on hierarchical structural model, in: *Proceedings of the International Symposium on Computer-Based Medical Systems*, IEEE, 2010, pp. 78–84.
- [14] Y. Deng, Y. Wang, P. Chen, J. Yu, A hierarchical model for automatic nuchal translucency detection from ultrasound images, *Comput. Biol. Med.* 42 (6) (2012) 706–713.
- [15] J. Moratalla, K. Pintoff, R. Minekawa, R. Lachmann, D. Wright, K. Nicolaides, Semi-automated system for measurement of nuchal translucency thickness, *Ultrasound Obstet. Gynecol.* 36 (4) (2010) 412–416.
- [16] E. Supriyanto, L. Wee, T. Min, Ultrasonic marker pattern recognition and measurement using artificial neural network, in: *Proceedings of the International Conference on Signal Processing*, 2010, pp. 35–40.
- [17] J. Park, M. Sofka, S. Lee, D. Kim, S. Zhou, Automatic nuchal translucency measurement from ultrasonography, in: *Proceedings of the International Conference on Signal Processing*, Vol. 8151 of *Lecture Notes in Computer Science*, Springer, 2013, pp. 243–250.
- [18] R. Sonia, V. Shanthi, Image classification for ultrasound fetal images with increased nuchal translucency during first trimester using SVM classifier, *Res. J. Appl. Sci. Eng. Technol.* 9 (2) (2015) 113–121.
- [19] A. Anzalone, G. Fusco, F. Isgrò, E. Orlandi, R. Prevete, G. Sciortino, D. Tegolo, C. Valenti, A system for the automatic measurement of the nuchal translucency thickness from ultrasound video stream of the foetus, in: *Proceedings of the International Symposium on Computer-Based Medical Systems*, IEEE, 2013, pp. 239–244.
- [20] G. Sciortino, E. Orlandi, C. Valenti, D. Tegolo, Wavelet analysis and neural network classifiers to detect mid-sagittal sections for nuchal translucency measurement, *Image Anal. Stereol.* 35 (2) (2016) 105–115.
- [21] M. Shensa, The discrete wavelet transform: wedding the à trous and Mallat algorithms, *IEEE Trans. Signal Process.* 40 (10) (1992) 2464–2482.
- [22] M. González-Audicana, X. Otazu, O. Fors, A. Seco, Comparison between Mallat's and the 'à trous' discrete wavelet transform based algorithms for the fusion of multispectral and panchromatic images, *Int. J. Remote Sens.* 26 (3) (2005) 595–614.
- [23] R. Jain, R. Kasturi, B. Schunck, *Machine Vision*, McGraw-Hill Inc., New York, NY, USA, 1995 ISBN:0-07-032018-7.
- [24] S. Szénási, Segmentation of colon tissue sample images using multiple graphics accelerators, *Comput. Biol. Med.* 51 (2014) 93–103.
- [25] C. Loizou, T. Kasparis, T. Lazarou, C. Pattichis, M. Pantziaris, Manual and automated intima-media thickness and diameter measurements of the common carotid artery in patients with renal failure disease, *Comput. Biol. Med.* 53 (2014) 220–229.
- [26] G. Loy, A. Zelinsky, Fast radial symmetry for detecting points of interest, *IEEE Trans. Pattern Anal. Mach. Intell.* 25 (8) (2003) 959–973.
- [27] P. Soille, *Morphological Image Analysis: Principles and Applications*, Springer-Verlag, Berlin Heidelberg, 2004 ISBN: 978-3-540-42988-3.